This article has been accepted for publication in a future issue of this journal, but has not been fully edited. Content may change prior to final publication. Citation information: DOI 10.1109/TIFS.2018.2799421, IEEE Transactions on Information Forensics and Security

Accurate and Efficient Image Forgery Detection Using Lateral Chromatic Aberration

Owen Mayer, *Student Member, IEEE,* Matthew C. Stamm, *Member, IEEE*

***Abstract*—In copy-and-paste image forgeries, where image content is copied from one image and pasted into another, inconsistencies in an imaging feature called lateral chromatic aberration (LCA) are intrinsically introduced. In this paper, we propose a new methodology to detect forged image regions that is based on detecting localized LCA inconsistencies. To do this, we propose a statistical model that captures the inconsistency between global and local estimates of LCA. We then use this model to pose forgery detection as a hypothesis testing problem and derive a detection statistic, which we show is optimal when certain conditions are met. To test its detection efficacy, we conduct a series of experiments that demonstrate our proposed methodology significantly outperforms prior art and addresses deficiencies of previous research. Additionally, we propose a new and efficient LCA estimation algorithm. To accomplish this we adapt a block matching algorithm, called diamond search, which efficiently measures the LCA in a localized region. We experimentally show that our proposed estimation algorithm reduces estimation time by two orders of magnitude without introducing additional estimation error.**

***Index Terms*—Lateral Chromatic Aberration, Multimedia Forensics, Forgery Detection, Efficient Block Matching**

I. Introduction

DIGITAL multimedia forensics has shown that statistical features intrinsic to images can be used to identify altered images [1]. An important type of alteration to detect is the copy-paste image forgery, where image content is copied from one image and pasted into another, or same, image. This operation is often done to maliciously change the meaning or context of an image by inserting or concealing objects in it. Prior research has shown that copy-paste forgeries can be detected by finding localized inconsistencies in intrinsic image features such as traces of resampling [2], [3], JPEG compression [4]–[6], contrast enhancement [7], median filtering [8], [9], and sensor noise [10]. Additionally, techniques that work by finding duplicate image blocks [11], [12], and by matching SIFT features [13], [14], have been developed to detect copy-move image forgeries, where image content is pasted into the same image that it was cut from. Work in [15] proposes a statistical framework for the fusion of such forgery detection features.

In this work, we propose a new forgery detection technique that uses lateral chromatic aberration (LCA) as an intrinsic imaging feature to expose image regions that have been falsified through copy-paste or copy-move type manipulations. Lateral chromatic aberration is a phenomenon that occurs in optical imaging systems. It arises due to a lens's inability to focus all wavelengths of a single light ray to a single location on a sensor and, as a result, the focal locations of different wavelengths are displaced laterally from each other in the image [16]. These displacements are often imperceptible to the human eye, but can be measured computationally. When a copy-paste or copy-move image forgery is made, the LCA inherent to the copied content is transferred into the falsified region. This creates a detectable inconsistency within the LCA patterning of the forged image. Forgeries are detected by comparing local observations of LCA displacement vectors to a global displacement model of displacement, then identifying localized inconsistencies.

Johnson and Farid first introduced the idea that LCA inconsistency can be used to detect image forgeries [17]. Research by Yerulshamy and Hel-Or has shown that purple fringing aberrations, a sensor induced aberration whose characterization also captures a subset of LCA effects, can also be used to detect image forgeries [18]. Work in [19] shows that LCA model parameters can be used to identify the image's source camera model. Additionally, research has shown that an image's lateral chromatic aberration can be anti-forensically modified to avoid forgery detection [20], and that these anti-forensic modifications can also be detected [21].

To detect image forgeries, Johnson and Farid proposed using the absolute value of the angle between between local and global LCA displacement vectors as a detection statistic [17]. However, their method suffers when the local and global displacement vectors differ in magnitude only and not angle. This occurs, for example, when image content is moved radially inward or outward from the image optical center. Additionally, their method is undefined when image content is cut from near the image optical center, where the local LCA displacements have no magnitude and thus no angle.

An additional drawback of the technique proposed by Johnson and Farid is that their method of estimating LCA is computationally demanding, resulting in long processing times for forensic investigation of even single images. To address this, Gloe et al. developed a technique to estimate LCA in an image in a more runtime efficient manner [22]. They accomplish this by computing local estimates of LCA displacement by performing a search over possible displacements between blocks across color channels for the one that maximizes similarity, then fitting a parameterized global model to these local estimates. While their method achieves marked

O. Mayer and M. C. Stamm are with the Department of Electrical and Computer Engineering, Drexel University, Philadelphia, Pennsylvania 19104 USA e-mail: om82@drexel.edu, mstamm@coe.drexel.edu

This material is based upon work supported by the National Science Foundation under Grant No. 1553610.

Source code for this work can be found at misl.ece.drexel.edu/downloads or the project git repository gitlab.com/mislgit/misl-lca-tifs

This article has been accepted for publication in a future issue of this journal, but has not been fully edited. Content may change prior to final publication. Citation information: DOI 10.1109/TIFS.2018.2799421, IEEE Transactions on Information Forensics and Security

efficiency gains over that of Johnson and Farid [22], it still incurs a high computation cost due to the high number of similarity calculations incurred by the displacement search.

In this work we propose a new detection methodology that more accurately detects forged image regions using lateral chromatic aberration. In our methodology, we propose a statistical model that describes the inconsistency between local and global estimates of lateral chromatic aberration. This statistical model captures two distributions; one for LCA inconsistency in authentic image regions, which we model as a random noise variable that is Gaussian, independent and identically distributed with near-zero mean, and another distribution that describes LCA in forged regions with similar assumed properties and with a forgery related bias. Then, using our proposed statistical model, we pose forgery detection as a hypothesis testing problem and derive a detection statistic, which is thresholded to make a detection decision. When our assumptions hold true, this detector forms an optimal decision region.

To test the efficacy of the detection algorithm, we conduct a series of experiments on a publicly available image database. We find that our algorithm significantly outperforms prior art in general scenarios. We find that our proposed algorithm is able to detect image forgery scenarios where angular-error based methods fare no better than random chance, such as in a radial-forgery scenario. Another experiment shows that there are significant image areas where our method is able to measure inconsistency between local and global estimates of LCA, but angular-error based methods cannot. We experimentally characterize the effects of local LCA estimation resolution and forgery size on forgery detection performance. We also show that our LCA-based method outperforms other forgery detection methods based on purple fringing aberrations.

Furthermore, we propose a new local LCA estimation algorithm that reduces the number of similarity calculations performed in the displacement search. This is done by adapting for LCA an algorithm optimized for MPEG motion-vector estimation [23], called the diamond search. In our experimental results section, we show that our proposed LCA estimation algorithm achieves two orders of magnitude time-efficiency gains over Gloe et al.'s method, without introducing additional estimation error.

This paper extends our initial study in [24] on the use of a statistical testing based framework for LCA forgery detection. We extend our previous work by deriving a new form of our forgery detection metric. This new derivation explicitly accounts for inherent variation in the number of keypoints in forged regions, and leads to non-trivial improvements in detection performance as shown in the experimental results. We conduct experiments on a larger, more comprehensive and publicly available image database [25], demonstrating efficacy of LCA based forgery detection on a substantially larger dataset and on a diverse set of imaging scenarios. We also characterize the affect of forgery size on detection performance, as well as the affects of choice of algorithm parameters such as estimation resolution. Additionally, we propose a new algorithm that estimates LCA in digital images in a computationally efficient manner. This proposed algorithm

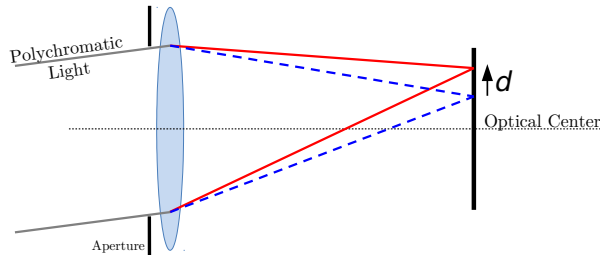

Fig. 1. Ray diagram of lateral chromatic aberration. Two rays of polychromatic light from a single point source are shown. The focal location of the red channel is laterally offset from the focal location of the blue channel by displacement vector $\mathbf{d}$.

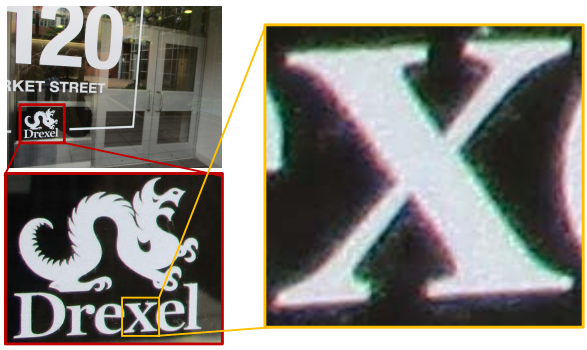

Fig. 2. Example of lateral chromatic aberration in an image. The red and blue LCA "fringes" become visible in the right inset, which is scaled 50 times larger than the original. This unaltered, JPEG compressed image was taken by a Canon Powershot ELPH 160 camera.

improves the run-time performance of LCA forgery detection significantly, allowing an investigator or researcher to conduct large scale investigations, such as the ones presented in this paper, on a reasonable time scale.

The remainder of this paper is organized as follows. In Sec. II we describe the background and theory of lateral chromatic aberration and how it is used to detect image forgeries. In Sec. III we propose a new, efficient algorithm to obtain local estimates of lateral chromatic aberration, called diamond search. In Sec. IV we develop a new method that determines if a region of an image is forged or authentic. We do this by proposing a statistical model of LCA inconsistency, posing forgery detection as a hypothesis test, and deriving an optimal detection metric. In Sec. V we conduct a series of experiments that compares the computation efficiency and estimation error of our proposed LCA estimation algorithm, and compare to the method proposed by Gloe et al. [22]. Finally, in Sec. VI we conduct a series of experiments that tests the efficacy of our proposed forgery detection metric, and compare to methods proposed by Johnson and Farid [17], in our initial conference paper related to this work [24], and to the purple fringing based method in [18].

II. Background

When light passes through a lens, it is focused onto a camera's imaging sensor through refraction. The refractive index of glass, however, is dependent upon the wavelength of the light passing through it [16]. This causes different

This article has been accepted for publication in a future issue of this journal, but has not been fully edited. Content may change prior to final publication. Citation information: DOI 10.1109/TIFS.2018.2799421, IEEE Transactions on Information Forensics and Security

color components of light, originating from the same point source in a scene, to be focused onto laterally offset locations on the sensor. This phenomenon, known as lateral chromatic aberration, is shown Fig. 1. An example of how LCA manifests in an image is shown in Fig. 2, where red and blue fringes become visibly apparent near the edges of the image.

Since the angle of refraction is also dependent on a light ray's angle of incidence with the lens, the distance between the focal locations for different wavelengths of light becomes greater as the distance from the optical center increases. As a result, LCA causes an image's color channels to be related through a relative expansion or contraction about the image's optical center. That is, one color channel of the image can be thought of as an expanded or contracted version of another color channel.

The effects of LCA are characterized by the mapping that relates the location of a point $\mathbf{r} = (r_x, r_y)^\mathsf{T}$ in a reference color channel to its corresponding location in a comparison color channel $\mathbf{c} = (c_x, c_y)^\mathsf{T}$. Johnson and Farid proposed the following parametric model of this mapping [17]

$$\mathbf{c} = f(\mathbf{r}, \boldsymbol{\theta}) = \alpha(\mathbf{r} - \boldsymbol{\zeta}) + \boldsymbol{\zeta}, \tag{1}$$

where α is the expansion coefficient, and $\boldsymbol{\zeta} = (\zeta_x, \zeta_y)^\mathsf{T}$ is the location of the image's optical center, and $\boldsymbol{\theta} = (\alpha, \boldsymbol{\zeta})^\mathsf{T}$ is the parameter tuple for the model $f(\cdot)$. We note that the optical center of an image is not necessarily its geometric center.

Additionally, it is often useful to think about the *displacement vector* between corresponding reference and comparison channel points $\mathbf{r}$ and $\mathbf{c}$

$$\mathbf{d}(\mathbf{r}, \boldsymbol{\theta}) = \mathbf{c} - \mathbf{r} = \alpha(\mathbf{r} - \boldsymbol{\zeta}) + \boldsymbol{\zeta} - \mathbf{r}. \tag{2}$$

Displacement $\mathbf{d}(\cdot, \cdot)$ is a function of both the reference location, $\mathbf{r}$, as well as the chromatic aberration model parameters $\boldsymbol{\theta}$. The displacement vector describes the spatial offset between a focal point in a reference color channel relative to its corresponding point in a comparison color channel. The description of LCA displacement is completed by specifying the reference and comparison color channels, which we often leave out of the notation to be described in the text. An example of an authentic image's LCA displacement vector field is shown in Fig. 3a. A distinct patterning is observed with all displacement vectors pointing radially outward (inward, if the expansion coefficient were less than 1) from the image optical center, growing in magnitude as distance from the optical center increases.

In addition to lateral chromatic aberrations, other types of chromatic aberrations can be found in digital images including axial chromatic aberration and purple fringing aberration. Axial chromatic aberration is a type of optical aberration, like LCA. It arises due to corresponding focal points in different color channels being focused out of plane with respect to each other. This results in an effect where, locally, one color channel appears out of focus with respect to the other.

Purple fringing aberration (PFA) is another type of chromatic aberration and is used in [18] as a feature for forgery detection. PFA appears as blue-purple halos around edges of objects in an image. PFA is attributed to a number of sensor effects including 1) electron overflow in CCD sensors, 2) sensitivity of the CCD sensor to non-visible light, and 3) light impingement on neighboring cells from refraction of the sensor micro-lens [18]. In this work, we solely consider optically induced lateral chromatic aberrations as a feature for forgery detection.

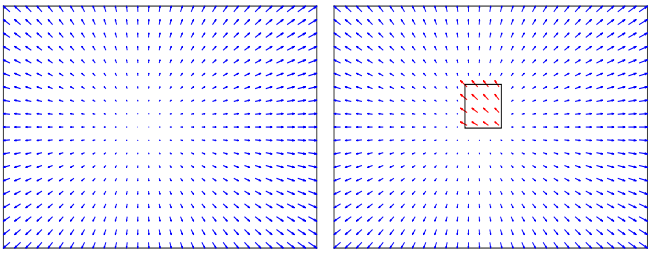

(a) Original Image LCA (b) Forged Image LCA

Fig. 3. Lateral chromatic aberration (LCA) displacement fields in (a) an authentic image and (b) a forged image. The LCA displacement in the forged region (in red) is inconsistent with the LCA in the rest of the image.

A. Lateral Chromatic Aberration Estimation

In practice, the expansion coefficient and optical center of an image are typically unknown and must be estimated. Johnson and Farid proposed estimating these model parameters by using the inverse mapping $f^{-1}(\cdot, \boldsymbol{\theta}^*)$ of (1) to undo the effects of LCA [17]. The estimated parameter values $\boldsymbol{\theta}^*$ are chosen as those that maximize the mutual information $\mathcal{I}(\cdot\,;\cdot)$ between the reference channel $\mathcal{R}$ and a corrected version of the comparison channel $\mathcal{C}$ that has been warped by the inverse mapping f^{-1}, i.e.

$$\boldsymbol{\theta}^* = \arg\max_{\boldsymbol{\theta}} \mathcal{I}\left(f^{-1}(\mathcal{C}, \boldsymbol{\theta}); \mathcal{R}\right) \tag{3}$$

The optimal parameter values $\boldsymbol{\theta}^*$ are found by performing an exhaustive search over a large set of candidate values. While this approach can accurately estimate the true LCA parameters in an image, its computational cost renders it impractical for use in large-scale forensic settings.

B. Efficient Estimates Based on Local Displacements

To address the problem of high computational cost, Gloe et al. proposed a more computationally efficient technique to estimate the model parameters [22]. It operates by obtaining estimates of the LCA displacement vector $\hat{\mathbf{d}}(\mathbf{r})$ at many keypoints $\mathbf{r}$ located throughout an image. The optimal model parameters are then identified by performing a least-squares fit of the estimated displacement vectors to the model (2) using an iterative Gauss-Newton method.

Local estimates of the LCA displacement vector $\hat{\mathbf{d}}(\mathbf{r})$ are obtained by searching for a $W \times W$ block $\mathbf{C}(x, y)$ in the comparison channel centered at location $(x, y)^\mathsf{T}$ that maximizes similarity with an equivalently sized block $\mathbf{R}(r_x, r_y)$ in the reference channel centered around $\mathbf{r}$, such that

$$\hat{\mathbf{d}}(\mathbf{r}) = \underset{(m,n)\in\{-\Delta,\ldots,\Delta\}}{\arg\max} S(\mathbf{R}(r_x, r_y), \mathbf{C}(r_x+m, r_y+n)) \tag{4}$$

where the similarity $S(\cdot)$ is measured using the correlation coefficient. The algorithm searches for the displacement

This article has been accepted for publication in a future issue of this journal, but has not been fully edited. Content may change prior to final publication. Citation information: DOI 10.1109/TIFS.2018.2799421, IEEE Transactions on Information Forensics and Security

(m, n) that relates two maximally similar blocks across color channels, and attributes this displacement to LCA. To enable a search over fractional pixel displacements, both blocks are upsampled by a factor of u. This search is performed exhaustively over a set of displacements between $-\Delta$ and Δ. That is, Δ defines the largest allowable displacement in the x or y direction, and bounds the search space.

This method implicitly assumes that LCA displacement is constant over the $W \times W$ block, and thus W should be chosen to be sufficiently small so that this assumption holds. The window size W should also be chosen to be sufficiently large so that an accurate assessment of similarity can be made. Furthermore, the keypoint locations are chosen to be corner points using Shi and Tomasi's minimum-eigenvalue corner metric [26]. Using corner points ensures there is sufficient spatial gradient in both the x and y directions to properly resolve LCA in both spatial dimensions.

In addition to determining local estimates of LCA, Gloe et al. proposed a method for determining an estimate for the global model parameters of LCA. This is done by finding the tuple $\boldsymbol{\theta}^*$ that minimizes the sum squared error between a sequence of local estimates and the parameterized model:

$$\boldsymbol{\theta}^* = \underset{\boldsymbol{\theta}}{\operatorname{argmin}} \sum_{i=1}^{N} \left\| \hat{\mathbf{d}}(\mathbf{r}_i) - \mathbf{d}(\mathbf{r}_i, \boldsymbol{\theta}) \right\|_2^2 \tag{5}$$

using the N local displacements estimated in the image for a specified reference and comparison channel pair. The minimization is solved using an iterative Gauss-Newton method [22], [27]. This provides an estimate for the LCA model parameters in an image, provided that the forgery area is sufficiently small and does to significantly bias the minimization. Since determining many local estimates is more run-time efficient than the Johnson and Farid's estimation method, it is able to more quickly determine an accurate estimate for global model parameters [22].

C. Forgery Detection

In a copy-paste forgery, image content in a region of an image is moved to another image. This includes any inherent chromatic aberration that exists within the copied region. When looking at the LCA displacement field of a copy-paste forgery, the falsified region becomes readily apparent as a region that does not agree with the global model of the rest of the image, as shown in Fig. 3b.

Johnson and Farid proposed using the absolute angular difference between a LCA displacement determined locally to a displacement determined by the global model as a forgery detection feature [17].

$$\phi = \frac{1}{N} \sum_{i=1}^{N} |\angle \hat{\mathbf{d}}(\mathbf{r}_i) - \angle \mathbf{d}(\mathbf{r}_i, \boldsymbol{\theta}^*)| \tag{6}$$

This angular difference is averaged over pixels in a region and compared to a threshold. Image patches with an average angular error less than the threshold are considered true to the global model, and thus authentic. Patches that result in angular error greater than a threshold are considered to be from a falsified region.

III. Efficient Estimation of Local LCA

Long and inefficient processing times are a burden to forensic investigation. Gloe et al. developed a technique to estimate local lateral chromatic aberration, which has been shown to reduce the computational expense of LCA-based forensic investigations [22]. However, their method still incurs a high computation cost that is prohibitive in practical and large scale forensic scenarios. A majority of the incurred computational expense is due to the high number of similarity calculations required to estimate local displacements. In this section, we propose a new, computationally efficient algorithm that reduces the number of similarity calculations required to accurately estimate local LCA displacements. To do this, we use an efficient block matching algorithm, called *diamond search*. By adapting the diamond search algorithm, which was originally developed for efficient MPEG encoding [23], we are able to significantly reduce the computational cost and time of using lateral chromatic aberration as a feature for forgery detection.

A. Diamond Search

In Gloe et al.'s method for estimating local LCA displacement, a small block of one color channel is compared to a displaced block of another channel using a similarity measure (e.g. correlation coefficient). The local estimate for lateral chromatic aberration at image location $\mathbf{r}$ is the displacement $\hat{\mathbf{d}}(\mathbf{r}) = (m_{max}, n_{max})^\intercal$ that results in maximum similarity between the two blocks across color channels. The variables m and n correspond to shifts in the x and y directions, respectively. To find this displacement, an exhaustive search is performed over all possible m and n that are bounded by $-\Delta$ and $+\Delta$ in increments of $\frac{1}{u}$. The variable u is an upsample factor that allows for fractional displacement, and also roughly introduces a notion of measurement resolution. In this exhaustive search $(2u\Delta + 1)^2$ possible displacements, and thus that many similarity calculations, are required to find a local LCA displacement.

The total number of similarity calculations in an exhaustive search can be quite large (e.g. 961 for $u = 5$, $\Delta = 3$). Furthermore, the high number of similarity calculations is compounded by the need to estimate local LCA at many locations within an image in a forensic investigation. Since similarity measures themselves are complex operations, LCA displacement estimation is a time consuming process, especially when using an exhaustive search.

We find that the use of an efficient block matching algorithm significantly reduces the number of similarity calculations required to estimate local lateral chromatic aberration. Consequently, by reducing the number of similarity calculations, a significant decrease in computation time is achieved. In particular, we adapt for LCA the diamond search algorithm, which was developed by Zhu and Ma for motion vector estimation in MPEG encoding [23].

The search for local LCA displacement is analogous to the search for motion vectors used in MPEG encoding; local LCA estimation searches for the lateral displacement that maximizes block similarity across color channels, whereas motion vector

This article has been accepted for publication in a future issue of this journal, but has not been fully edited. Content may change prior to final publication. Citation information: DOI 10.1109/TIFS.2018.2799421, IEEE Transactions on Information Forensics and Security

estimation searches for the lateral displacement that maximizes block similarity across time frames.

By utilizing the diamond search method, only a subset of all possible displacements are tested for similarity while achieving a similar estimate. This is accomplished by iteratively choosing a small number of displacement test points, which ultimately converge upon the displacement of maximum similarity. The result of fewer similarity calculations is an overall reduction in the computational expense and increase in time efficiency of estimating local LCA displacements.

At each step of the diamond search algorithm, similarity is tested at multiple displacements that are designated by the search patterns in Fig. 4. Similarity can be determined by any measure of similarity for gray-scale images, such as the correlation coefficient [28] or mutual information. Initially, the Large Diamond Search Pattern (LDSP) is used and centered about $(m, n) = (0, 0)$. Similarity is measured between color channel blocks with the comparison block displaced by all (m, n) designated by the LDSP. The LDSP is then recentered at the displacement which resulted in maximum local similarity, and all new displacements designated by the LDSP are tested (there will be some overlap of the LDSP with its previous position). This recentering process is repeated until the center of the LDSP maintains maximum similarity. Then, the Small Diamond Search Pattern (SDSP) is centered at the new LDSP center. The displacement (m_{max}, n_{max}) is designated by the SDSP that results in maximum similarity.

A more explicit algorithm is as follows:

Algorithm 1 Diamond Search

1: **repeat**
2: **if** First repetition **then**
3: Center LDSP at $(m, n) = (0, 0)$
4: **else**
5: Center LDSP at displacement that resulted in maximum similarity
6: **end if**
7: Measure similarity at displacements as designated by the LDSP and that are within the search space
8: **until** Maximum similarity found at the LDSP center
9: Center SDSP at LDSP center
10: Measure similarity at displacements designated by SDSP
11: $(m_{max}, n_{max}) \leftarrow$ SDSP displacement that results in maximum similarity
12: **return** $\hat{\mathbf{d}} = (m_{max}, n_{max})^{\mathsf{T}}$

B. Keypoint Selection

In a forensic investigation, local LCA displacement estimates are made at many corner points throughout an image. To select corner points, we use Shi and Tomasi's minimum-eigenvalue corner point metric [26]. Using corner points are necessary to ensure that LCA displacement is measured accurately in both the x and y directions. Since the local estimation technique is a spatial average of LCA over an image block, estimates at nearby corner points within the block add very little LCA information while adding significant computation expense. To mitigate this, in the keypoint selection step we first segment the image into many small, non-overlapping blocks and select the largest corner point within each block among those whose corner metric exceed a threshold. Selecting corners block-wise ensures that local LCA measurements are distributed spatially within the image (i.e. to prevent clumping of corner points in texture-rich areas), without incurring undue computation cost.

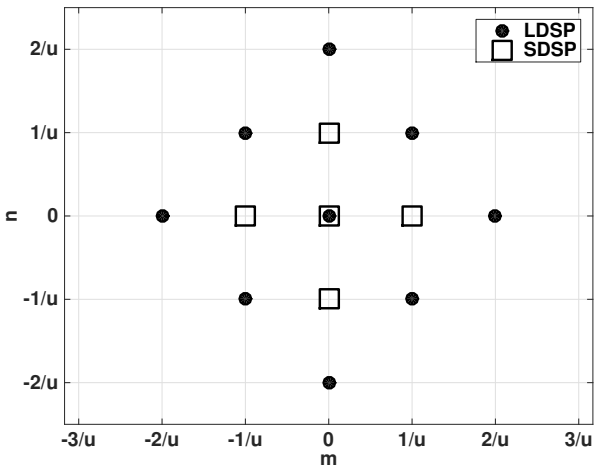

Fig. 4. Large Diamond Search Pattern (LDSP) and Small Diamond Search Pattern (SDSP).

IV. Accurate Forgery Detection

Forgeries are discovered by detecting the regions of an image where the local estimates of lateral chromatic aberration (LCA) deviate from the global LCA model of the image. Previously, researchers have proposed using the average absolute angular difference between local and global displacement vectors as a metric for inconsistency [17]. However this metric has several explicit shortcomings that result in inferior detection performance. To address this, we propose a new methodology that not only detects forgeries in the scenarios where previous detectors do not, but also improves detection performance in general scenarios.

A. Shortcomings of Existing Metrics

Here, we describe the shortcomings of the detection metric proposed by Johnson and Farid [17]. Johnson and Farid used the *average absolute angular difference* between local and global LCA displacements as an inconsistency metric:

$$\phi = \frac{1}{N} \sum_{i=1}^{N} |\angle \hat{\mathbf{d}}(\mathbf{r}_i) - \angle \mathbf{d}(\mathbf{r}_i, \boldsymbol{\theta}^*)| \tag{7}$$

where the N local displacement estimates, $\hat{\mathbf{d}}(\mathbf{r}_i)$, and global displacement estimates, $\mathbf{d}(\mathbf{r}_i, \boldsymbol{\theta}^*)$, are at corresponding points, $\mathbf{r}_i$, in a region of interest for $i \in \{1, \ldots, N\}$. N is the number of corner points found in the region. Large angles between the local and global LCA displacement vectors are indicative of forgeries, and thus when this metric is sufficiently large then a forgery is declared. Johnson and Farid suggest a 60° threshold.

This article has been accepted for publication in a future issue of this journal, but has not been fully edited. Content may change prior to final publication. Citation information: DOI 10.1109/TIFS.2018.2799421, IEEE Transactions on Information Forensics and Security

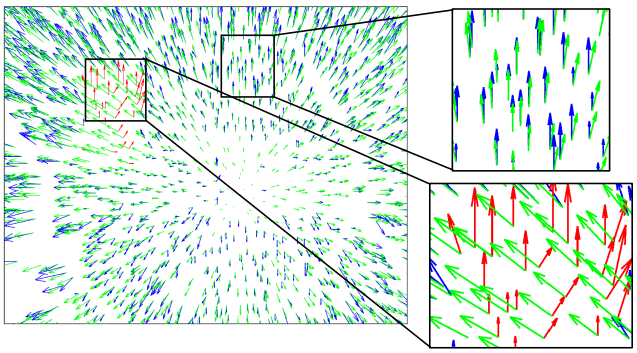

Fig. 5. Lateral chromatic aberration displacement field in a forged image. Global model (green), local estimates in authentic regions (blue), and local estimates in forged regions (red). The top right inset highlights that authentic local estimates noisily approximate the global model, whereas the local estimates in a forged region, as in the bottom right inset, are additionally biased by a forgery related offset.

There are, however, two deficiencies of this approach that our proposed metric overcomes. First, when image content originates from a location the near the image optical center, an angular error metric is unable to render a decision on it. This is because LCA at locations near the optical center is small and so local displacements have zero-magnitude when near the optical center. Local displacement estimates with zero magnitude have undefined angle. Thus, when forged image content is sourced from near the image optical center, angle based detectors are unable to render a decision on them. This is a significant deficiency since image content near the center tends to contain salient visual information that may likely be the subject of a forgery.

Second, Johnson and Farid's metric fails in forgery scenarios where the LCA local to the forged region differs from the global model in magnitude, but not angle. This occurs, for example, when image content is copied and pasted radially inward or outward towards the image optical center. An angular error based metric is unable to resolve LCA inconsistencies in such scenarios, resulting in an ineffective classification methodology.

Furthermore, the metric proposed by Johnson and Farid is a heuristic approach. That is, this type of approach may not form an optimal decision region, and therefore cannot be guaranteed to make the best detection decision.

B. Proposed Model of LCA Inconsistency

In our approach, we first observe that local LCA estimates noisily fit the global model estimate. This can be seen in Fig. 5, which shows the the local LCA displacement field for a forged image, as well as the global model. The local LCA displacement estimates fit, but do not exactly match, the global LCA model. We propose a new model that captures this inconsistency between local and global LCA with two possible distributions; one for inconsistency in authentic regions and the other for forged regions. From the two distributions, we frame forgery detection as a hypothesis testing problem. Using the hypothesis test, we derive a detection statistic that decides if an image region has been falsified through copy-paste forgery.

As seen in Fig. 5, the local estimates of lateral chromatic aberration displacement can be viewed as noisy approximations of the global model. In this figure, the local estimates in the authentic regions closely approximate the the global model, and any inconsistency between the global model and authentic local estimates we attribute to observational noise. This observational noise arises from the discrete and quantized nature of the local estimation method, compression artifacts, other chromatic aberration artifacts like purple fringing aberrations, as well as scene-dependent biases.

We propose a new model that incorporates a model mismatch term, $\mathbf{n} = (n_x, n_y)^\mathsf{T}$ that, when added to the scaled reference location of the global model, captures the discrepancy between a local estimate of LCA to the global model:

$$\hat{\mathbf{d}}(\mathbf{r}) = \alpha(\mathbf{r} + \mathbf{n} - \boldsymbol{\zeta}) + \boldsymbol{\zeta} - \mathbf{r} \tag{8}$$

Where $\hat{\mathbf{d}}(\mathbf{r})$ is the local estimate for LCA displacement at pixel location $\mathbf{r}$ in the reference color channel, determined by our proposed estimation method in Sec. III. The right side of the equation is the global model of LCA introduced earlier (2), with expansion coefficient α and optical center $\boldsymbol{\zeta}$, and the observational noise term $\mathbf{n}$ added to the scaled reference location.

We model this noise term as an independent and identically distributed (IID) Gaussian random variable with a near-zero mean $\boldsymbol{\mu}_0$ and covariance $\boldsymbol{\Sigma}$. Fig. 6a shows a histogram of this noise term calculated from an unaltered, JPEG compressed image. A Gaussian distribution is fit to the observed noise, and is shown in red. It can be seen in Fig. 6a that, by eye, the Gaussian fit reasonably captures the empirical noise distribution. In Fig. 6b, Quantile-Quantile (Q-Q) and scatter plots are shown of the observed noise for both x and y components as well as different reference-comparison color channel pairings. The Q-Q plots are referenced to the fit Gaussian distribution and appear linear for each component, save a few outliers on either end, suggesting that a multivariate Gaussian distribution is appropriate in this case. The scatter plots show that across directional components (x vs. y) of the distributions are roughly uncorrelated, whereas some correlations exist across color pairings (gr vs. gb). We also consider each noise observation to be spatially independent of each other as well as identically distributed. In practice, these assumptions may not be exact in every case (e.g. due to mismatch between the estimated and true LCA global model) but we assume them to be sufficiently close going forward.

In a forged image region, the local estimates of LCA have an additional discrepancy we denote the *forgery offset*, $\boldsymbol{\delta} = (\delta_x, \delta_y)^\mathsf{T}$. As a result, the local estimate of LCA displacement $\hat{\mathbf{d}}(\mathbf{r})$ in a forged region is

$$\hat{\mathbf{d}}(\mathbf{r}) = \alpha(\mathbf{r} + \mathbf{n} + \boldsymbol{\delta} - \boldsymbol{\zeta}) + \boldsymbol{\zeta} - \mathbf{r} \tag{9}$$

Again, $\hat{\mathbf{d}}(\mathbf{r})$ is the local estimate for LCA displacement at a reference location $\mathbf{r}$ in the image. The expansion coefficient α and optical center $\boldsymbol{\zeta}$ are the parameters of the global model. The observational noise $\mathbf{n}$ has the same mean and covariance as in the unaltered scenario. The forgery offset arises from the copy-paste operation, where image content, and consequently LCA, is displaced from one image location to another. Thus

This article has been accepted for publication in a future issue of this journal, but has not been fully edited. Content may change prior to final publication. Citation information: DOI 10.1109/TIFS.2018.2799421, IEEE Transactions on Information Forensics and Security

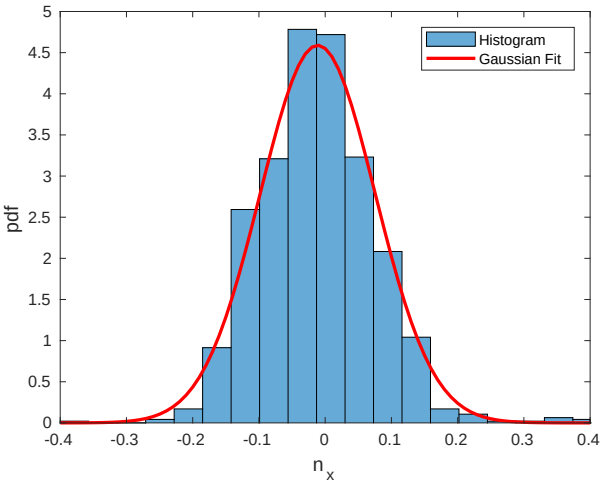

(a) LCA Inconsitency Histogram

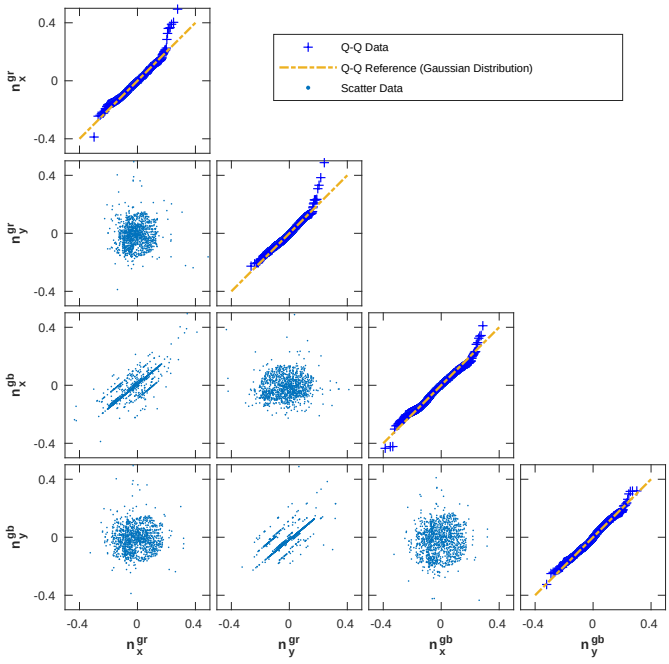

(b) Inconsistency Q-Q and Scatter Plots by Component

Fig. 6. Normalized histogram, Quantile-Quantile (Q-Q) and scatter plots of observational noise components in an unaltered Kodak M1063 image. The plots are is calculated from local estimates of green-to-red (gr) and green-to-blue (gb) LCA at $N = 1094$ locations.

the resultant LCA in the forged region appears to come from another reference location which is related by the forgery offset $\boldsymbol{\delta}$. The effect of the forgery offset can be see in the lower right inset of Fig. 5, where the local estimate vectors are biased away from the global model.

In order to capture the differences between the local estimates and global model, we introduce a new function, $\mathbf{e}(\mathbf{r}) = (e_x(\mathbf{r}), e_y(\mathbf{r}))^\mathsf{T}$, called *LCA inconsistency*, which we define as the Cartesian difference vector between the local and global LCA estimate of displacement, $\hat{\mathbf{d}}$ and $\mathbf{d}$ respectively, at a point $\mathbf{r}$ in the reference channel, scaled by the inverse of the global LCA expansion coefficient:

$$\mathbf{e}(\mathbf{r}) = \alpha^{-1}\left(\hat{\mathbf{d}}(\mathbf{r}) - \mathbf{d}(\mathbf{r}, \boldsymbol{\theta})\right) \tag{10}$$

Solving for $\mathbf{e}$ in an authentic image region yields

$$\begin{aligned}\mathbf{e}(\mathbf{r}) &= \alpha^{-1}\left((\alpha(\mathbf{r} + \mathbf{n} - \boldsymbol{\zeta}) + \boldsymbol{\zeta}) - (\alpha(\mathbf{r} - \boldsymbol{\zeta}) + \boldsymbol{\zeta})\right) \\ &= \mathbf{n}\end{aligned} \tag{11}$$

and in a forged region yields

$$\begin{aligned}\mathbf{e}(\mathbf{r}) &= \alpha^{-1}\left((\alpha(\mathbf{r} + \mathbf{n} + \boldsymbol{\delta} - \boldsymbol{\zeta}) + \boldsymbol{\zeta}) - (\alpha(\mathbf{r} - \boldsymbol{\zeta}) + \boldsymbol{\zeta})\right) \\ &= \mathbf{n} + \boldsymbol{\delta}\end{aligned} \tag{12}$$

We can see that LCA inconsistency captures purely observational noise at locations in authentic regions. In forged regions, however, we see that there is the forgery offset in addition to observational noise. Therefore, by measuring LCA inconsistency in an image region, we can gain insight into whether the region is forged by how far the inconsistency vector deviates from the mean observational noise $\boldsymbol{\mu}_0$. It often suffices to think of the mean observational noise as being zero, but in practice any misestimation of the global model parameters can add bias to the noise. Allowing the observational noise to be non-zero gives slight improvement to detection accuracy.

So far we have not explicitly stated which reference and comparison channel, to use. In most images, there are three color channels - red, green, and blue - and thus three possible reference-comparison channel pairings. Since we would like to exploit all LCA information between channels, we use two pairs with green as the reference color channel and red and blue as the comparison color channels.[1] This is done by concatenating two 2D LCA inconsistency vectors, each of which are determined from one reference-comparison channel pair, into a single 4D vector.

$$\mathbf{e}(\mathbf{r}) = \begin{bmatrix} e_x^{gr}(\mathbf{r}) \\ e_y^{gr}(\mathbf{r}) \\ e_x^{gb}(\mathbf{r}) \\ e_y^{gb}(\mathbf{r}) \end{bmatrix} = \begin{bmatrix} \frac{1}{\alpha^{gr}}\left(\hat{d}_x^{gr}(\mathbf{r}) - d_x^{gr}(\mathbf{r}, \boldsymbol{\theta}^{gr})\right) \\ \frac{1}{\alpha^{gr}}\left(\hat{d}_y^{gr}(\mathbf{r}) - d_y^{gr}(\mathbf{r}, \boldsymbol{\theta}^{gr})\right) \\ \frac{1}{\alpha^{gb}}\left(\hat{d}_x^{gb}(\mathbf{r}) - d_x^{gb}(\mathbf{r}, \boldsymbol{\theta}^{gb})\right) \\ \frac{1}{\alpha^{gb}}\left(\hat{d}_y^{gb}(\mathbf{r}) - d_y^{gb}(\mathbf{r}, \boldsymbol{\theta}^{gb})\right) \end{bmatrix} \tag{13}$$

The superscripts gr and gb denote green-to-red (i.e. using the green channel as reference, and red as comparison) and green-to-blue LCA, respectively. Furthermore, since the true global model of LCA is typically unknown for an image, we estimate it for each of the color channel pairs using the iterative Guass-Newton method described in Sec. II-B substituting $\boldsymbol{\theta}^*$ for $\boldsymbol{\theta}$ in the equation above.

C. Optimal Detection

In order to determine if an image region contains forged content, we begin by measuring a sequence of N LCA inconsistency vectors $\{\mathbf{e}(\mathbf{r}_1), \mathbf{e}(\mathbf{r}_2), \ldots, \mathbf{e}(\mathbf{r}_N)\}$ from the N corner points in that region, and use this sequence to construct a hypothesis test. We assume the sequence of LCA inconsistency to be either purely observational noise that is IID Gaussian about mean $\boldsymbol{\mu}_0$, and thus not indicative of forged content,

[1]The third possible pair, red-to-blue LCA displacement, adds no new information since it can be determined by the addition of red-to-green and green-to-blue LCA.

This article has been accepted for publication in a future issue of this journal, but has not been fully edited. Content may change prior to final publication. Citation information: DOI 10.1109/TIFS.2018.2799421, IEEE Transactions on Information Forensics and Security

or alternatively the sequence of LCA inconsistency contains a forgery offset with IID Gaussian distribution about mean $\boldsymbol{\mu}_0 + \boldsymbol{\delta}$ and thus indicative of a forgery. We use the log-likelihood ratio to construct the optimal detection statistic, which is compared to a threshold to render a decision.

From the two forms of the LCA inconsistency model shown in (11) and (12), we form the following two hypotheses:

$$H_0: \quad \mathbf{e}(\mathbf{r}) \sim \mathcal{N}(\boldsymbol{\mu}_0, \boldsymbol{\Sigma}) \qquad Authentic \tag{14}$$

$$H_1: \quad \mathbf{e}(\mathbf{r}) \sim \mathcal{N}(\boldsymbol{\mu}_0 + \boldsymbol{\delta}, \boldsymbol{\Sigma}) \qquad Forged \tag{15}$$

The mean of the observational noise $\boldsymbol{\mu}_0$ and covariance of the observational noise $\boldsymbol{\Sigma}$ are not known apriori and are estimated from all LCA inconsistency vectors outside of the region.

The following equation specifies the likelihood $\mathcal{L}(\cdot)$ of mean $\boldsymbol{\mu}$ and covariance $\boldsymbol{\Sigma}$ conditioned on an observed sequence of N independent and identically distributed LCA inconsistency vectors $\{\mathbf{e}(\mathbf{r}_1), \mathbf{e}(\mathbf{r}_2), \ldots, \mathbf{e}(\mathbf{r}_N)\}$:

$$\begin{aligned}
&\mathcal{L}\left(\boldsymbol{\mu}, \boldsymbol{\Sigma} | \mathbf{e}(\mathbf{r}_1), \ldots, \mathbf{e}(\mathbf{r}_N)\right) \\
&= f(\mathbf{e}(\mathbf{r}_1), \ldots, \mathbf{e}(\mathbf{r}_N) | \boldsymbol{\mu}, \boldsymbol{\Sigma}) \\
&= \frac{|\boldsymbol{\Sigma}|^{-N/2}}{(2\pi)^{2N}} \exp\left\{ -\frac{1}{2} \sum_{i=1}^{N} \left(\mathbf{e}(\mathbf{r}_i) - \boldsymbol{\mu}\right)^T \boldsymbol{\Sigma}^{-1} \left(\mathbf{e}(\mathbf{r}_i) - \boldsymbol{\mu}\right) \right\}
\end{aligned} \tag{16}$$

where $f(\cdot)$ is the probability density function of a sequence of N independent and identically distributed 4D Gaussian random variables.

We construct a log-likelihood ratio using the likelihood function (16) with the two hypotheses in (15):

$$\begin{aligned}
&\log\left(\frac{f\left(\mathbf{e}(\mathbf{r}_1), \ldots, \mathbf{e}(\mathbf{r}_N) | \boldsymbol{\mu}_0 + \boldsymbol{\delta}, \boldsymbol{\Sigma}\right)}{f\left(\mathbf{e}(\mathbf{r}_1), \ldots, \mathbf{e}(\mathbf{r}_N) | \boldsymbol{\mu}_0, \boldsymbol{\Sigma}\right)} \right) \\
&\quad = -\frac{1}{2} \sum_{i=1}^{N} (\mathbf{e}_i - \boldsymbol{\mu}_0 - \boldsymbol{\delta})^{\mathsf{T}} \boldsymbol{\Sigma}^{-1} (\mathbf{e}(\mathbf{r}_i) - \boldsymbol{\mu}_0 - \boldsymbol{\delta}) \\
&\qquad + \frac{1}{2} \sum_{i=1}^{N} (\mathbf{e}(\mathbf{r}_i) - \boldsymbol{\mu}_0)^{\mathsf{T}} \boldsymbol{\Sigma}^{-1} (\mathbf{e}(\mathbf{r}_i) - \boldsymbol{\mu}_0)
\end{aligned} \tag{17}$$

Applying a threshold to (17) forms an optimal, Neyman-Pearson detector. Algebraic reduction yields a simplified form of the optimal detector:

$$N\left(\bar{\mathbf{e}} - \boldsymbol{\mu}_0\right)^{\mathsf{T}} \boldsymbol{\Sigma}^{-1} \boldsymbol{\delta} \underset{H_1}{\overset{H_0}{\lessgtr}} \tau \tag{18}$$

where $\bar{\mathbf{e}}$ is the sample average of the N LCA inconstancy vectors $\mathbf{e}(\mathbf{r}_i), i \in \{1, \ldots, N\}$ measured in a region, and τ is a decision threshold, such that when the detection score is less than τ we accept the null hypothesis H_0 and declare the region to be authentic. Alternatively, if the detection score on the left side of (18) is greater than τ, we reject the null hypothesis and declare the region to be forged.

We note that the optimality of this detector requires the assumptions of $\mathbf{e}(\mathbf{r})$ to be Gaussian and IID. In practice, these assumptions may not be exact and as a result the detector may not always form the optimal decision region. This may arise due to mismatch between the estimated LCA global model and true global model, which may contain 2nd or higher order terms than used in (1). However, empirical results in Sec. VI, which show markedly improved detection performance over prior art, suggest that these assumptions may be close enough in practice.

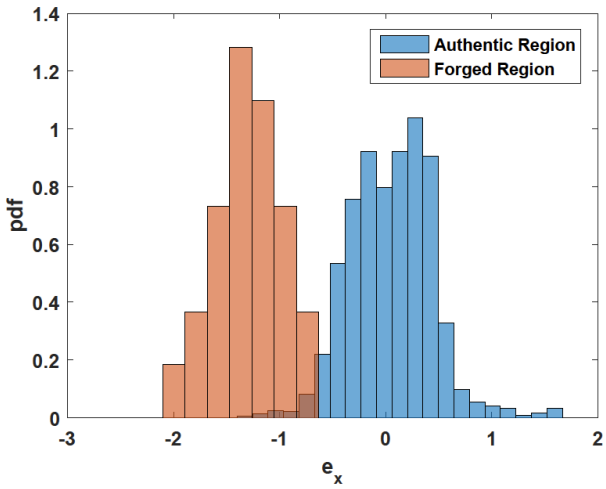

Fig. 7. Normalized histograms of the horizontal component of green-to-red LCA inconsistency in a forged image. We model both distributions as Gaussian, where the inconstancy in the forged region has a forgery-related bias. The forgery was created by copying a 512x512 pixel block from a Sony DSC-H50 image and randomly pasting into a Olympus Mju 1050 SW image.

The form of this detector differs slightly from our previous derivation in [24] where the scaling by N is not included. In our previous derivation, we had implicitly assumed that the number of LCA inconsistency observations N in a region is constant and thus absorbed into the decision threshold. In practice, the number of inconsistency vectors in a region is dictated by the number of corner points that are found, which are scene dependent and not controllable. So, by allowing N to scale, this form is able to account for variations in the number of corner points in a region, which leads to a superior result as shown in our experimental validation.

Furthermore, without knowledge of the LCA in the forged region's source image, the forgery offset $\boldsymbol{\delta}$ is unknown. In its place, we use its maximum-likelihood estimate $\hat{\boldsymbol{\delta}}$. Since LCA inconsistency in forged regions has a Gaussian distribution with mean $\boldsymbol{\mu}_0 + \boldsymbol{\delta}$, we determine the forgery offset estimate with the following equation.

$$\hat{\boldsymbol{\delta}} = \frac{1}{N} \sum_{i=1}^{N} \mathbf{e}(\mathbf{r}_i) - \boldsymbol{\mu}_0 = \bar{\mathbf{e}} - \boldsymbol{\mu}_0 \tag{19}$$

Substituting $\hat{\boldsymbol{\delta}}$ for $\boldsymbol{\delta}$ in (18) yields:

$$N\left(\bar{\mathbf{e}} - \boldsymbol{\mu}_0\right)^{\mathsf{T}} \boldsymbol{\Sigma}^{-1} \left(\bar{\mathbf{e}} - \boldsymbol{\mu}_0\right) \underset{H_1}{\overset{H_0}{\lessgtr}} \tau \tag{20}$$

which is the final form of our proposed detection metric.

The resulting metric above takes the form of a scaled (by N) Mahalanobis distance. The Mahalanobis distance provides a metric of dissimilarity between the LCA inconsistency in a region and purely observational noise. Notably, the inverse covariance matrix $\boldsymbol{\Sigma}^{-1}$ term takes into account any inherent component correlations that may exist in the authentic inconsistency distribution, which aids in detection if those same

This article has been accepted for publication in a future issue of this journal, but has not been fully edited. Content may change prior to final publication. Citation information: DOI 10.1109/TIFS.2018.2799421, IEEE Transactions on Information Forensics and Security

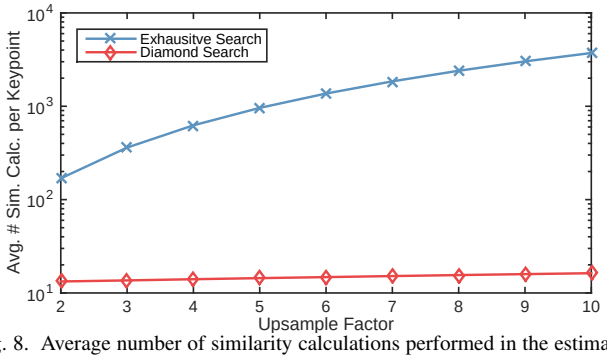

Fig. 8. Average number of similarity calculations performed in the estimation of local LCA displacement at image locations in the "Schoner Muehle" and "Reed" image sets. The proposed Diamond Search method reduces the number of similarity calculations by over two orders of magnitude for upsample factors 6 and greater.

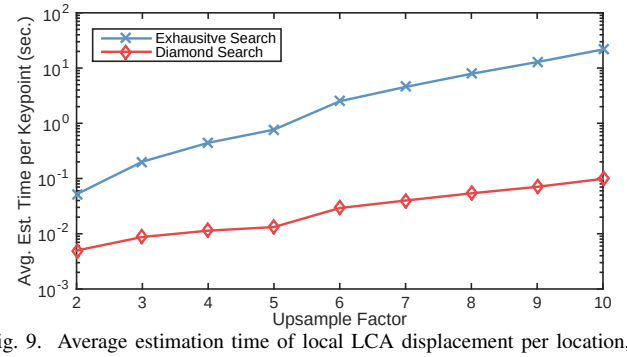

Fig. 9. Average estimation time of local LCA displacement per location, in seconds, in images from the "Schoner Muehle" and "Reed" image sets. The proposed Diamond Search method reduces estimation time by over two orders of magnitude for upsample factors 6 and greater.

correlations do not exist in the forged region. Additionally, the scaling term N provides some confidence proportional to the number of observations; it allows small forgery offsets to be detected provided there are enough observations, and prevents single outliers from causing false alarms.

V. Computational Efficiency Experiments

Fast and accurate estimates of local lateral chromatic aberration (LCA) are essential to the practical forensic investigator. Here, we evaluate the computational efficiency and accuracy performance of our proposed LCA estimation algorithm compared to the method presented by Gloe et al. [22]. In one experiment, we estimated local LCA displacements in natural, JPEG compressed images from the publicly available Dresden Image Database [25]. We compared the number of similarity calculations performed by each method in the estimation of local LCA, as well as elapsed processing time. We found that our proposed method reduces the number of similarity calculations by at least one, and typically two orders and reduces computation time at least one, and typically two orders of magnitude compared to Gloe et al.'s method, achieving substantial time savings.

In another experiment, we evaluated estimation error introduced by each method. We compared local estimates to known LCA in a synthetically generated checkerboard image. We found that our method incurs no additional error over Gloe et al.'s method, and does so in a much more run-time efficient manner.

A. Computation and Run-Time Efficiency

In our first experiment, we tested the computational efficiency improvement of using our proposed diamond search (DS) algorithm, compared to the exhaustive search (ES) method proposed by Gloe et al. We started with a database of 434 images from the "Schoner Muehle" and "Reed" image sets of the Dresden Image Database. These image sets were chosen for their diversity of texture and texture location, and contain unaltered images from 27 camera models. We randomly chose one image from each camera model. In each image, 100 corner points were chosen at random among those that exceeded a threshold of 0.005 as determined by the Shi and Tomasi corner metric [26]. In total, we estimated LCA at 2700 corner locations.

We then compared the elapsed time and number of similarity calculations performed in the estimation of local LCA displacement at each corner point. For the estimation of LCA, we used a window size of $W = 64 \times 64$, maximum displacement $\Delta = 3$, and upsample factor u varied from 2 to 10. We used the correlation coefficient [28] as a similarity measure with the green color channel as the reference channel and the red color channel as the comparison channel.

Fig. 8 summarizes the average number of similarity calculations performed by each algorithm in the estimation of a single local displacement. We see that at all upsample factors our proposed diamond search (DS) method estimates local LCA with fewer similarity calculations than Gloe et al.'s exhaustive search (ES) method. For example, at an upsample factor of 5 our method estimates local LCA with an average of 14.4 similarity calculations, which is 1.5% of the 961 similarity calculations used in the exhaustive search method. Furthermore, at an upsample factor of 10, our method estimates local LCA with an average of 16.3 similarity calculations, which is 0.4% of the 3721 similarity calculations used by the exhaustive search method.

Fig. 9 summarizes the mean computation time of estimating a single local displacement for each algorithm.[2] At each upsample factor the DS algorithm achieves an improvement in run-time efficiency over the ES method. At an upsample factor of 5, the ES estimates a single displacement in an average of 0.77 seconds, whereas the DS completes 59 times faster in an average of 0.013 seconds. At an upsample factor of 10, the ES estimates a single displacement in 21.96 seconds compared to 0.099 seconds for the DS, 221 times faster. As an example of the scale of improvement in a forgery investigation, measuring local LCA in 1000 images with 1000 corners each would take over 8 months using the exhaustive search using an upsample factor of 10, compared to just one day and 4 hours using the diamond search.

[2]Experiments were conducted on a 3.4 GHz Intel i7-4770 CPU using MATLAB 2015b.

Source code for this work can be found at misl.ece.drexel.edu/downloads or the project git repository gitlab.com/mislgit/misl-lca-tifs

This article has been accepted for publication in a future issue of this journal, but has not been fully edited. Content may change prior to final publication. Citation information: DOI 10.1109/TIFS.2018.2799421, IEEE Transactions on Information Forensics and Security

TABLE I
MEAN EUCLIDEAN ERROR (PIXELS) OF LOCAL LCA DISPLACEMENTS ESTIMATED IN A SYNTHETIC CHECKERBOARD IMAGE

	Upsample Factor, u								
	2	3	4	5	6	7	8	9	10
Clean Image									
ES	0.050	0.026	0.015	0.013	0.010	0.010	0.009	0.008	0.006
DS	0.050	0.026	0.015	0.013	0.010	0.010	0.009	0.008	0.006
Noisy, Blurred, and JPEG Compressed Image									
ES	0.138	0.080	0.063	0.059	0.060	0.060	0.057	0.057	0.057
DS	0.138	0.080	0.063	0.059	0.060	0.060	0.057	0.057	0.057

B. Estimation Error

In the second experiment, we measured the estimation error incurred by our algorithm and compare to Gloe et al.'s algorithm. To do this, we generated a synthetic checkerboard image with induced, ground truth lateral chromatic aberration. We then calculated local estimates in the image using our proposed method and the one proposed by Gloe et. al, and compare to the ground-truth LCA.

The checkerboard image has 100×100 pixel blocks, 20 blocks across and 15 blocks down forming a 4000×3000 pixel image. The blocks alternate between black and white creating 1131 corner points, excluding those along the image edge. We induced artificial LCA into the image using the method presented in our previous work [20], which algorithmically shifts and scales the color channels in an image to alter it's LCA. We introduced green-to-red LCA with an optical center at the center of the image, with an expansion coefficient of 1.00032, simulating an Agfa Sensor 530s image. In order to simulate a real-world imaging scenario, we created a second image with additive Gaussian white noise with variance $1/255$, Gaussian blurring with variance 0.25, and JPEG compression with quality factor 95 and 4:2:0 chroma subsampling. The use of chroma subsampling reduces the spatial resolution in the chroma domain, which likely introduces additional error in the compressed image LCA.

Table I shows the average Euclidean error between the local estimate and ground truth using Gloe et. al's exhaustive search (ES) method and our proposed diamond search (DS) method. At an upsample factor of 2, both the diamond search and exhaustive search methods have an average estimation error of 0.05 pixels in the clean image and 0.138 pixels in the noisy, blurry, and compressed image. At an upsample factor of 10, both diamond search and exhaustive search methods have an average estimation error of 0.006 pixels in the clean image and 0.057 pixels in the noisy, blurry and compressed image. We see that estimation error decreases as the upsample factor increases. Intuitively, this is due to the higher upsample factor allowing for more precise local LCA estimates. Furthermore, the error incurred is the same between all methods. That is, there is no accuracy penalty incurred by using our more efficient approach. The local estimation accuracy was worse in the noisy, blurry and compressed image than in the clean version. This finding suggests that image quality plays an important role in local LCA estimation accuracy and, by extension, forgery detection accuracy.

In addition, we assessed the error between the two methods by comparing the local LCA estimate values from the timing experiment in Sec. V-A, which uses captured images from the Dresden Image Database. At an uspample factor of 10 (the most sensitive measurement resolution), only 1 of the 2700 local estimates was different between the diamond and exhaustive search methods. The distance between the two estimates was 0.3 pixels. Without knowing the ground truth it is impossible to know which estimate is more correct. The average disagreement between the two methods over all 2700 estimates is $0.3/2700 = 1.1 \times 10^{-4}$ pixels per local estimate. Since this is well below the expected error in even the clean and uncompressed synthetic image, we conclude that any disagreement between the methods is negligible.

The results of the experiments in Sec. V-A and the above experiments introduce a notion of accuracy-versus-efficiency trade off. An increase in upsample factor reduces estimation error, but also significantly increases computational time. Similarly, a decrease in upsample factor decreases computation time but also has the effect of increasing estimation error.

VI. FORGERY DETECTION EXPERIMENTS

To test the efficacy of our proposed forgery detection methodology, we conducted a series of experiments under various forgery scenarios, and compare to the performance of the angular error metric proposed by Johnson and Farid [17] as well as the metric we proposed in previous work (MS'16) [24], which doesn't adjust for the number of corner points.

We started with a database of 16961 unaltered, JPEG compressed images from the publicly available Dresden Image Database [25]. Forgeries were created by copying image content from a *source location* in a *source image* and pasting into a *destination location* in a *destination image*. The source and destination images may be the same image, in the case of a copy-move scenario. Blocks of size 512×512 were used to create the forgeries, and we required there to be 10 corner points within the source location since LCA cannot be measured in smooth regions.

To detect forgeries, we first determined corner points at which to measure local LCA. To do this, we divided the image into 72×72 pixel blocks, and within each block specified the local estimate location to be the corner point that achieved the largest corner metric, as defined by the Shi and Tomasi metric, among those that exceeded a threshold of 0.005.

Second, we estimated local LCA at each specified location using the procedure described in Sec. III. We used window a size of $W = 64 \times 64$, maximum displacement Δ = 3, and upsample factor $u = 5$. The green color channel was used as the reference channel, with both red and blue channels as comparison. Global LCA estimates are determined for each test image by using the Gauss-Newton method described in Sec. II-B to determine estimates of the green-to-red and green-to-blue LCA model parameters.

The detection method was then applied in regions of interest within the test image. For forged images, we specified the region of interest to be the destination location of the forged content. In authentic images, we defined multiple regions

This article has been accepted for publication in a future issue of this journal, but has not been fully edited. Content may change prior to final publication. Citation information: DOI 10.1109/TIFS.2018.2799421, IEEE Transactions on Information Forensics and Security

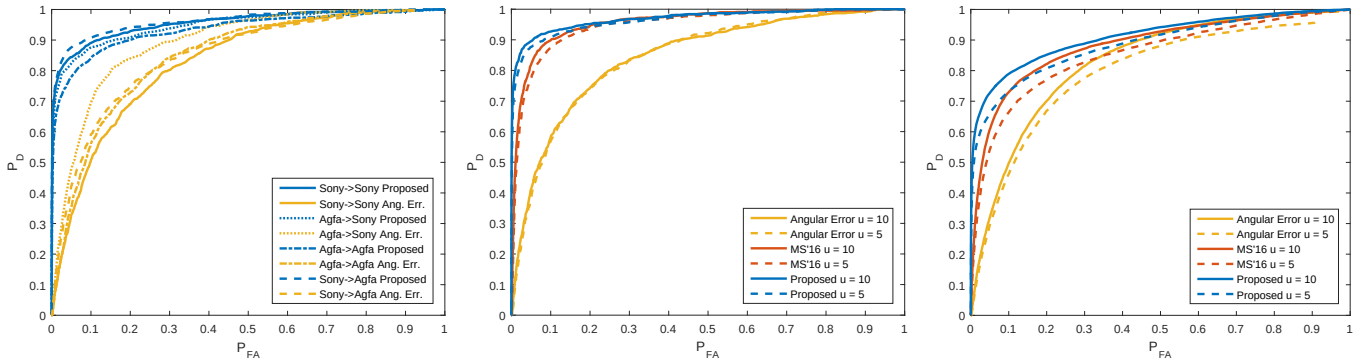

(a) Images from DSC-H50 and Sensor530s Cameras (b) Copy from DSC-H50 and Paste to Sensor530s (c) All Cameras in Image Database

Fig. 10. Receiver operator characteristic curves of copy-paste forgery detection in forgery scenarios where source and destination image and location are chosen randomly. These curves provide a comparison between our proposed metric, one proposed in our previous work (MS'16) and the angular error metric proposed by Johnson and Farid.

TABLE II
DETECTION RATES OF RANDOM COPY PASTE FORGERIES COPIED FROM SONY DSC-H50 AND PASTED INTO AGFA SENSOR530S IMAGES

	$u = 5$			$u = 10$		
P_{FA}	0.01	0.05	0.10	0.01	0.05	0.10
Proposed	0.76	0.87	0.91	0.80	0.90	0.93
MS'16	0.44	0.77	0.87	0.49	0.82	0.90
Ang. Err.	0.10	0.38	0.57	0.12	0.41	0.59

TABLE III
DETECTION RATES OF RANDOM COPY PASTE FORGERIES ON ENTIRE IMAGE DATABASE

	$u = 5$			$u = 10$		
P_{FA}	0.01	0.05	0.10	0.01	0.05	0.10
Proposed	0.52	0.66	0.73	0.59	0.73	0.79
MS'16	0.23	0.54	0.66	0.28	0.61	0.72
Ang. Err.	0.07	0.29	0.46	0.08	0.32	0.50

of interest of size 512×512, which span the image with 50% overlap. This region specification was chosen to directly compare the efficacy of our proposed metric with Johnson and Farid's on known forged regions.

A. Randomized Copy and Paste Locations

We tested the efficacy of our proposed detection metric in generalized forgery scenarios by randomly selecting the source and destination images, as well as source and destination locations to create a forgery. By randomly selecting copy and paste locations, we make no assumptions on location tendencies of a forger.

Fig. 10 shows receiver operator characteristic (ROC) curves of our proposed metric, the metric we used in previous work (MS'16), and the angular error metric proposed by Johnson and Farid. We tested on forged images created on various subsets of the image database.

In the first scenario, we restricted the source and destination images to be from either a Sony DSC-H50 or Agfa Sensor 530s camera. These camera models were chosen for exhibiting strong LCA characteristics. We create 1000 forgeries for each of the four possible source-destination camera model permutations. The ROC curves for the four cases are shown in Fig. 10a for our proposed metric and the angular error metric. At a false alarm rate of 0.05, our proposed metric achieved a positive detection rate between 0.78 and 0.87, whereas the angular error metric achieved a detection rate between 0.33 and 0.48, highlighting a significant improvement in detection rate when using our proposed metric. Generally, we found that cross-camera model forgeries are detected at higher rates, such as the "Sony→Agfa" case (i.e. cut from a Sony DSC-H50 image and paste to a Agfa Sensor530s image), than same-camera model forgeries, such as the "Agfa→Agfa" case, due to mismatch between the LCA global model parameters.

Fig. 10b shows the best case from the above scenario where source images come from a Sony DSC-H50 camera and destination images are from a Agfa Sensor 530s camera. Fig. 10b shows, in addition, comparisons to our previously proposed detection metric (MS'16) as well as using a higher upsample factor of 10. The corresponding numeric detection rate values for these curves at false alarm rates of 0.01, 0.05 and 0.1 are found in Table II. Our proposed algorithm significantly outperformed both our previously proposed metric and the angular error metric at all false alarm rates. Notably, at a lower false alarm rate of 1%, our proposed method achieved detection rates of 0.76 and 0.80 at upsample factors of 5 and 10 respectively, which improved detection rates over Johnson and Farid's angular error metric by 66 and 68 percentage points. Additionally, we note that increasing the upsample factor from 5 to 10 increased detection rates by 2 to 5 percentage points in all cases shown in Table II.

In a second scenario, we changed conditions on source and destination camera models and allowed any image in the database to be used as the source or destination image. We created 10000 such forgeries and also compared with a higher upsample factor of 10. Fig. 10c shows the ROC curves for this scenario and Table III contains the corresponding numeric detection rate values for these curves at false alarm rates of 0.01, 0.05 and 0.1. Again, our new proposed metric outperformed both our previously proposed metric and the angular error

This article has been accepted for publication in a future issue of this journal, but has not been fully edited. Content may change prior to final publication. Citation information: DOI 10.1109/TIFS.2018.2799421, IEEE Transactions on Information Forensics and Security

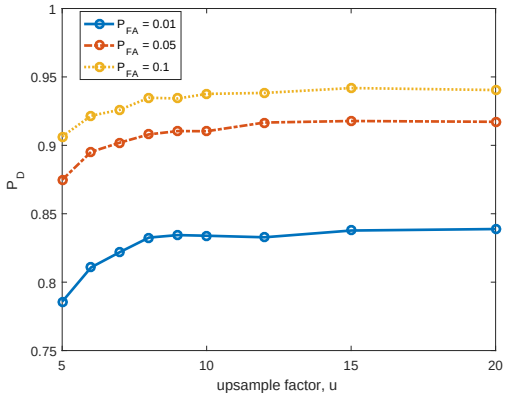

Fig. 11. Forgery detection rates by upsample factor. The upsample factor determines the search resolution of the local LCA estimation method, where a higher upsample factor yields a finer resolution and thus more accurate LCA estimates. The proposed forgery detection method was applied to a set of forgeries with the upsample factor varied. Increasing the upsample factor from 5 to 10 significantly increases detection rates, with little improvement at upsample factors greater than 10.

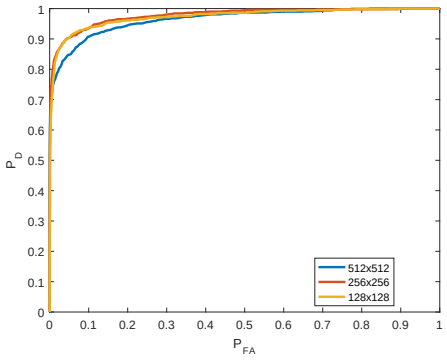

(a) Detection Rates by Forgery Size

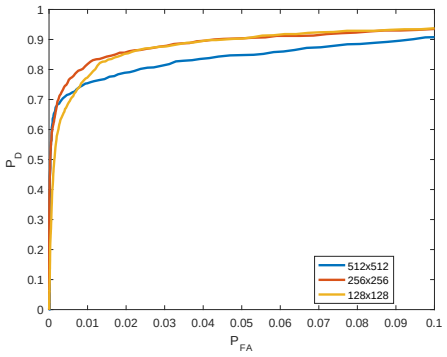

(b) Detail of Low P_{FA} region

Fig. 12. Receiver operator characteristic curves for the proposed detection method on forgeries of varying size. Forgeries were created by copying image content from Agfa Sensor530s images and were pasted into Sony DSC-H50 images, with randomly chosen copy and paste locations. Forged content that is large relative to the entire image, as with the 512×512 case, skew the global LCA model estimate and consequently degrade detection performance. Best detection performance is achieved at smaller forgery sizes of 128×128 and 256×256

metric at all false alarm rates. For example, at a false alarm rate of 1%, our proposed method achieved detection rates of 0.52 and 0.59 at upsample factors of 5 and 10 respectively, which improved detection rates over Johnson and Farid's angular error metric by 45 and 51 percentage points. Increasing the uspample factor from 5 to 10 increased detection rates by 1 to 7 percentage points in all cases shown in Table III. In this scenario the detection rates for all metrics were lower than in the first scenario. This is partly due to the fact that some of the cameras within the Dresden Image Database suppress chromatic aberration distortions, either computationally or through multi-element lens configurations. Other cameras may have worse image quality, which affects local LCA estimation (see experiments in Sec. V-B), or there may be other sources of non-LCA chromatic aberrations present, such as purple fringing aberrations, that may be causing unreliable LCA estimates.

Also of note is that the angular-error metric cannot render a decision on the forged and authentic regions that contain all zero-magnitude LCA displacements, since displacements with zero magnitude have undefined angle. As a result the angular-error metric cannot detect some of the forged regions or false-alarm on some authentic regions. This prevents the angular error ROC curve from achieving the 100%-detection-rate 100%-false-alarm-rate point that is typical of ROC curves.

B. Effect of Upsample Factor

In the first experiment, we found that forgery detection improved when the upsample factor was increased from 5 to 10. In this experiment we explore in depth the effect that the choice of upsample has on forgery detection. To do this, we repeated the copy-paste forgery detection experiment as performed in the previous experiment using different upsample factors. A higher upsample factor allows for finer resolution and precision of local LCA estimates, which should give more accurate forgery detection. To test this, we created an expanded set of 2500 forgeries by copying a 512×512 block from Agfa Sensor530s images pasted into Sony DSC-H50 images, using random copy and paste locations. We measured the forgery detection rates using our proposed algorithm, with local LCA estimation performed using upsample factors 5, 6, 7, 8, 9, 10, 12, 15, and 20.

TABLE IV
DETECTION RATES OF FORGERIES BY FORGED WINDOW SIZE

	$u = 10$		
P_{FA}	0.01	0.05	0.10
128×128	0.77	0.90	0.93
256×256	0.82	0.90	0.94
512×512	0.75	0.85	0.91

Fig. 11 shows the forgery detection rate versus the upsampling factor obtained at different false alarm rates. Generally, detection rates increase with the upsample factor. However, detection improvement flattens out at upsample factors greater than 10. Detection rates increased by 4.5 percentage points, from 78.6% to 83.4%, when doubling the upsample factor from u=5 to u=10 at a false alarm rate of 1%. However, detection rates only increased by 0.4 percentage points, from 83.4% to 83.8%, when doubling the upsample factor from u=10 to u=20 at a false alarm rate of 1%.

This article has been accepted for publication in a future issue of this journal, but has not been fully edited. Content may change prior to final publication. Citation information: DOI 10.1109/TIFS.2018.2799421, IEEE Transactions on Information Forensics and Security

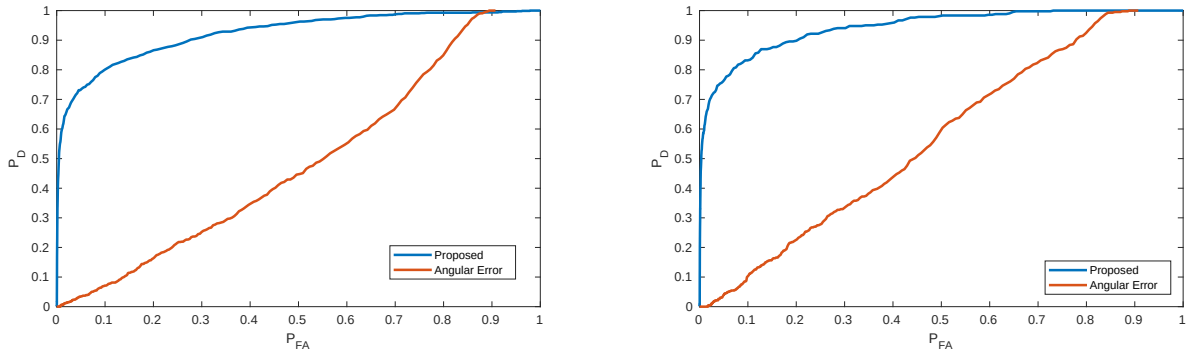

(a) Radial Forgery Sony DSC-H50 (b) Radial Forgery Agfa Sensor530s

Fig. 13. Reciever operator characteristic curves of radial copy-move forgeries. Forged images were created by moving a 512×512 block radially inwards toward the image optical center in (a) Sony DSC-H50 images and (b) Agfa Sensor 530s images. In this forgery scenario, forged local displacements are inconsistent with the global model in angle only, thus Johnson and Farid's angular error metric is ineffective.

TABLE V
DETECTION RATES ON RADIAL FORGERIES

	Sony DSC-H50			Agfa Sensor 530s		
P_{FA}	0.01	0.05	0.10	0.01	0.05	0.10
Proposed	0.59	0.73	0.80	0.61	0.76	0.83
Ang. Err.	0.01	0.04	0.07	0.00	0.04	0.10

C. Effect of Forgery Size

In this experiment, we tested how the size of the forged region affects the detection performance of our proposed algorithm. Since we cannot enforce nor predict the behavior of an image forger, it is important to understand the limitations of forgery detection methods. In images with small forged regions, there are likely fewer keypoints and as a result fewer opportunities to measure LCA. This can lead to diminished forgery detection performance. In images with large forged regions the statistics of the LCA in the forged regions will become non-negligible, skewing estimates of the global model. Poor global model estimates result in poor detection performance, due to an increase in the LCA inconsistency variance. Thus, there is likely a range of preferable forgery sizes for LCA based forgery detection for which any size smaller becomes too hard to detect, and any size larger causes poor global estimates.

To test the effect of forgery size on detection performance, we repeated the random copy and paste forgery experiment described in Sec. VI-A, varying the size of the copied content. We copied image content from Agfa Sensor530s images, and pasted into Sony DSC-H50 images, using random copy and paste locations, with forgery blocks of size 128×128, 256×256, and 512×512. For each size scenario, 1000 forgeries were made. We used a detection window size that matched the forgery size in each experiment, and a 16×16 corner point selection window to ensure a sufficient number of corner points for detection in the 128×128 case. An upsample factor of 10 was used.

Fig. 12 shows ROC curves for our proposed detection method in the different forgery size scenarios. At false alarm rates less than 40% these curves show that the smaller 128×128 and 256×256 cases have improved detection rates over the the larger 512×512 forgery size. This suggests that a forgery size of 512×512 is large enough to skew the global model estimates, leading to poor detection performance. Fig. 12b shows a detailed view of the ROC at false alarm rates below 10%. At false alarm rates below 1%, the 128×128 case shows decreased detection performance relative to the best case at 256×256. The inherent reduction in the number of corner points available is the likely cause of reduced forgery detection at the 128×128 size. The 256×256 has the highest detection rates at all false alarm rates.

D. Radial Forgery

In this experiment, we tested the efficacy of our proposed detection method in a difficult forgery scenario where local displacements are inconsistent with the global model in magnitude only, and not angle. This type of scenario is challenging to detect from a lateral chromatic aberration perspective. To do this, we start with the 372 Agfa Sensor30s images and 572 Sony DSC-H50 images from the database. Forgeries were made by copying image content from 100×100 pixels away from the image corners, and moving inwards along the radius to the image optical center, so that destination location is 100 pixels away from the optical center. This configuration, where forged LCA is inconsistent in magnitude only, is one of the most difficult forgery scenarios to detect in from a lateral chromatic aberration perspective. In total, 971 and 422 forgeries were created using from the Sony and Agfa images, where there were at least 10 corner points in the source region.

Fig. 13 shows the ROC curves for our proposed metric and the angular error metric. In both cases, our proposed metric significantly outperformed the angular error metric, which did little better than random chance, if at all. For example, at a false alarm rate of 0.05, our proposed metric achieved detection rates of 0.76 and 0.73 for the Agfa Sensor530s and Sony DSC-H50 radial forgeries respectively, whereas the angular error metric achieved detection rates of 0.04 and 0.04.

While a forger may not explicitly utilize such a scenario, this experiment highlights a significant deficiency in the de-

This article has been accepted for publication in a future issue of this journal, but has not been fully edited. Content may change prior to final publication. Citation information: DOI 10.1109/TIFS.2018.2799421, IEEE Transactions on Information Forensics and Security

TABLE VI
PROPORTION OF IMAGE AREA THAT HAS UNDEFINED LOCAL LCA ANGLE

Camera Model	Upsample Factor u = 5	u = 10
Agfa DC-504	0.33	0.15
Agfa DC-733s	0.60	0.34
Agfa DC-830i	0.42	0.21
Agfa Sensor505-x	0.70	0.35
Agfa Sensor530s	0.09	0.02
Canon Ixus55	0.47	0.22
Canon Ixus70	0.45	0.19
Canon PowerShotA640	0.06	0.01
Casio EX-Z150	0.67	0.43
FujiFilm FinePixJ50	0.59	0.27
Kodak M1063	0.37	0.17
Nikon CoolPixS710	0.55	0.31
Nikon D200	0.24	0.10
Nikon D70	0.40	0.20
Nikon D70s	0.38	0.20
Olympus mju1050SW	0.14	0.05
Panasonic DMC-FZ50	0.50	0.23
Pentax OptioA40	0.45	0.22
Pentax OptioW60	0.35	0.15
Praktica DCZ5.9	0.27	0.09
Ricoh GX100	0.80	0.56
Rollei RCP-7325XS	0.03	0.00
Samsung L74wide	0.20	0.07
Samsung NV15	0.16	0.04
Sony DSC-H50	0.11	0.03
Sony DSC-T77	0.29	0.11
Sony DSC-W170	0.40	0.14
Average	0.39	0.20

tection metric proposed by Johnson and Farid that our method overcomes.

E. Area of Undefined Angular Error

In this experiment, we estimated the area of images where local LCA estimates have no magnitude. If content were to be cut from this area during the creation of a forgery, the angular error metric would not be able to render a decision, since the local LCA in such areas have undefined angle.

To measure this area, we divided each image in our database into 72×72 blocks, and measured local LCA at the corner point within each block with the highest corner metric, among those that exceeded a threshold of 0.005 as determined by the Shi and Tomasi corner operator. Then, we calculated the proportion of blocks that have zero-magnitude LCA, for both green-to-red and green-to-blue LCA, to the total number of blocks that contain a corner point.

Table VI summarizes the proportion of image area that contains zero-magnitude LCA by camera model. The area proportion varied greatly; the smallest proportion is seen in the Rollei RCP-7325XS images, where 3% and 0% of the image area has zero-magnitude LCA for upsample factors 5 and 10 respectively, whereas the Ricoh GX100 images has 80% and 56% area with zero-magnitude LCA. Using a higher uspample factor reduces the zero-magnitude image area, since it allows for finer resolution measurement.

Many these cameras with high zero-magnitude area ratios employ some aberration compensation methods such as multi-element lenses with achromatic doublets, or low-dispersion

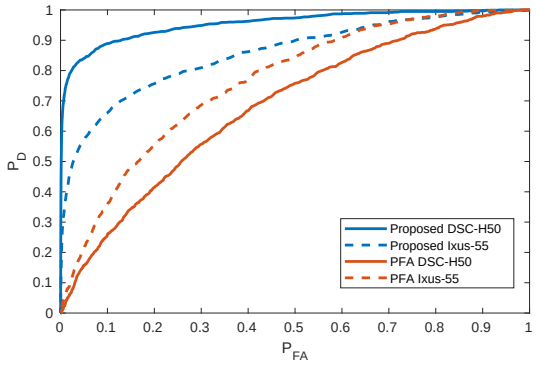

Fig. 14. Receiver operator characteristic for our proposed LCA-based forgery detection method and Yerulshalmy and Hel-Or's PFA-based forgery detection method. Forgeries were created using images from two different cameras, a Sony DSC-H50 and a Canon Ixus-55.

TABLE VII
PROPOSED AND PFA DETECTION RATES ON FORGERIES

	Sony DSC-H50			Canon Ixus-55		
P_{FA}	0.01	0.05	0.10	0.01	0.05	0.10
Proposed	0.73	0.84	0.89	0.36	0.57	0.67
Purp. Fring.	0.03	0.16	0.26	0.06	0.21	0.36

lenses. For example, the specification sheets of the Casio EX-Z150, Panasonic DMC-FZ50, and Ricoh GX100 cameras indicate that they contain such lens configurations, and these cameras contain high image areas with zero-magnitude LCA. Images from these types of cameras may not be suitable for LCA based forgery detection, since they suppress the LCA fingerprint.

F. Comparison to PFA-Based Forgery Detection

In addition to lateral chromatic aberrations, images may also contain purple fringing aberrations (PFA) which appear as blue-purple halos around object edges. Research has shown that localized inconsistencies in PFA can be used to detect image forgeries [18]. In this experiment, we compare the efficacy of our proposed LCA-based method to Yerushalmy and Hel-Or's PFA-based method of detecting forged image regions [18].

To conduct this experiment, we created a set of forgeries from images in the publicly available Dresden Image Database [25]. We created 1000 forgeries using Sony DSC-H50 images as source image and destination images, and another 1000 forgeries using Canon Digital Ixus-55 images as source and destination images. Forgeries were created by randomly choosing the source image and destination image, and copying and pasting a 512×512 image block from the source image into the destination image. The source and destination locations were chosen at random. The set of forgeries in the Sony DSC-H50 scenario are same used in the experiment in Sec VI-A. The Sony DSC-H50 camera were chosen for the presence of strong LCA traces in those images. Additionally, the Canon Ixus-55 camera was chosen for the strong presence of PFA traces in those images. This setup was used to give a favorable and unfavorable scenario for each

This article has been accepted for publication in a future issue of this journal, but has not been fully edited. Content may change prior to final publication. Citation information: DOI 10.1109/TIFS.2018.2799421, IEEE Transactions on Information Forensics and Security

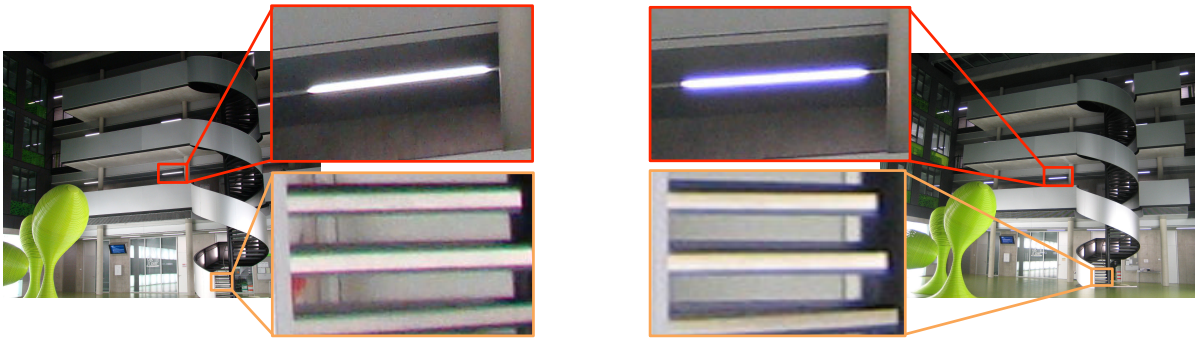

(a) Sony DSC-H50 (b) Canon Ixus-55

Fig. 15. Example images from (a) a Sony DSC-H50 camera and (b) a Canon Ixus-55 camera taken from the Dresden Image Database. In similar imaging environments, purple fringing aberrations are perceptible about the light fixtures (red inset) of the Canon image, but not the Sony image. In the Sony image, magenta and green chromatic aberrations are perceptible (orange inset), whereas the blue-purple and yellow fringing aberrations that are described in [18] are seen in the Canon image.

method. Fig. 15 shows examples of the PFA and LCA effects in a similar image for both cameras.

We calculated our proposed forgery detection metric on the forged region in each image. For the PFA method, we used an implementation of Yerushalmy and Hel-Or's method to detect forged image regions. Briefly, their method works by first identifying possible PFA events at object edges. Then, the color profile across each edge is examined in the xyY color space, and chroma excursions of significant distance towards the blue-purple region (x= 0.2, y = 0.1) are deemed PFA events. A direction and reliability measure are assigned to each PFA event. A sensor center location is then estimated from the PFA events, and PFA events that do not agree with the center estimate are assigned high inconsistency scores. A map of inconsistency scores is created and smoothed via spatial averaging. If an image region contains an inconsistency score above a forgery threshold, it is deemed a forged region. We used an implementation of this method provided by the authors of [18]. We modified this code to change the fixed forgery threshold to one that could be varied in order to measure detection performance at different false alarm rates. False alarm rates were assessed by measuring the detection statistic on all unaltered images from the Dresden Image Database. Each unaltered image was segmented into 512×512 blocks with 50% overlap, and the forgery detection metric was measured for each block. Only images with 300 or more corner points, and blocks with 10 or more corner points were assessed to ensure sufficient content to accurately measure LCA and PFA effects.

The receiver operator characteristics for our proposed LCA-based forgery detection method and Yerulshalmy and Hel-Or's PFA-based forgery detection method are shown in Fig. 14. In both forgery scenarios, our proposed method outperforms the PFA-based method. For example, at a 5% false alarm rate our proposed method detects 84% of the Sony DSC-H50 forgeries whereas the PFA-based method detects 16% of the forgeries, a 68 percentage point difference. For the Canon Ixus-55 forgeries, our method detects 57% of the forgeries whereas the PFA-based method detects 21% of the forgeries, a 36 percentage point difference.

Interestingly, our proposed method detects more of Sony DSC-H50 forgeries than the Canon Ixus-55 forgeries scenario, but the PFA-based method detects fewer Sony DSC-H50 forgeries than the Canon Ixus-55 forgeries. We attribute this result to the inherent differences in aberrations between the two camera models. That is, the LCA trace is stronger in the Sony DSC-H50 images than in the Canon Ixus-55 images, and the PFA trace stronger in the Canon Ixus-55 images than in the Sony DSC-H50 images. These effects are shown in Fig. 15. Our LCA-based method outperforms the PFA-based method in both tested scenarios. Additionally, the results of this experiment highlight that the efficacy of each detection method is tied to the strength of the respective fingerprint in the forgery.

VII. Conclusion

In this paper, we proposed a new methodology for detecting forged image regions using inconsistencies in lateral chromatic aberration (LCA). To do this, we proposed a statistical model that captures the inconsistency between global and local estimates of LCA. Using this statistical model, we pose forgery detection as a hypothesis testing problem, from which we derive a detection statistic that we show is optimal when LCA inconsistency is Gaussian and IID. We conduct a series of experiments that tests the efficacy of our proposed methodology and compare against previous metrics. In generalized forgery scenarios, we found that our proposed method improves detection rates by 51 percentage points over previous research at a 1% false alarm rate. When using image forgeries that exhibit strong LCA characteristics, our proposed method improves detection rates by 68 percentage points over previous research at a 1% false alarm rate. Additional experiments show that our proposed methodology overcomes significant deficiencies of previous research, namely when local estimates LCA are inconsistent in magnitude only and not angle, and when forged image content is cut from near optical center, which cannot be detected by methods in previous research. We also experimentally characterize the effect of upsample factor and forgery size on forgery detection performance. Furthermore, we proposed a new and efficient method to

estimate lateral chromatic aberration in a digital image. To do this we adapted for LCA a block matching algorithm, called diamond search, which efficiently finds the inter-channel spatial misalignment that is due to chromatic aberration in a localized region. We experimentally show that our proposed estimation algorithm reduces estimation time by two orders of magnitude without introducing additional estimation error.

ACKNOWLEDGMENT

The authors would like to thank I. Yerulshalmy and H. Hel-Or for providing the code that was used to conduct the purple fringing aberration analysis in the above experiments.

REFERENCES

[1] M. C. Stamm, M. Wu, and K. J. R. Liu, "Information forensics: An overview of the first decade," *Access, IEEE*, vol. 1, pp. 167–200, 2013.

[2] A. C. Popescu and H. Farid, "Exposing digital forgeries by detecting traces of resampling," *Signal Processing, IEEE Transactions on*, vol. 53, no. 2, pp. 758–767, 2005.

[3] M. Kirchner, "Fast and reliable resampling detection by spectral analysis of fixed linear predictor residue," in *Proceedings of the 10th ACM Workshop on Multimedia and security*. ACM, 2008, pp. 11–20.

[4] H. Farid, "Exposing digital forgeries from JPEG ghosts," *Information Forensics and Security, IEEE Transactions on*, vol. 4, no. 1, pp. 154–160, 2009.

[5] S. Ye, Q. Sun, and E.-C. Chang, "Detecting digital image forgeries by measuring inconsistencies of blocking artifact," in *Multimedia and Expo, 2007 IEEE International Conference on*. IEEE, 2007, pp. 12–15.

[6] T. Bianchi and A. Piva, "Image forgery localization via block-grained analysis of JPEG artifacts," *Information Forensics and Security, IEEE Transactions on*, vol. 7, no. 3, pp. 1003–1017, 2012.

[7] M. C. Stamm and K. J. R. Liu, "Forensic detection of image manipulation using statistical intrinsic fingerprints," *Information Forensics and Security, IEEE Transactions on*, vol. 5, no. 3, pp. 492–506, 2010.

[8] M. Kirchner and J. Fridrich, "On detection of median filtering in digital images," in *IS&T/SPIE Electronic Imaging*. International Society for Optics and Photonics, 2010, pp. 754 110–754 110.

[9] X. Kang, M. C. Stamm, A. Peng, and K. J. R. Liu, "Robust median filtering forensics using an autoregressive model," *IEEE Transactions on Information Forensics and Security*, vol. 8, no. 9, pp. 1456–1468, 2013.

[10] M. Chen, J. Fridrich, J. Lukáš, and M. Goljan, "Imaging sensor noise as digital x-ray for revealing forgeries," in *Proceedings of the 9th International Conference on Information Hiding*. Springer-Verlag, 2007, pp. 342–358.

[11] J. Fridrich, D. Soukal, and J. Lukáš, "Detection of copy-move forgery in digital images," in *in Proceedings of Digital Forensic Research Workshop*. Citeseer, 2003.

[12] A. C. Popescu and H. Farid, "Statistical tools for digital forensics," in *Proceedings of the 6th international conference on Information Hiding*. Springer-Verlag, 2004, pp. 128–147.

[13] I. Amerini, L. Ballan, R. Caldelli, A. Del Bimbo, and G. Serra, "A SIFT-based forensic method for copy–move attack detection and transformation recovery," *Information Forensics and Security, IEEE Transactions on*, vol. 6, no. 3, pp. 1099–1110, 2011.

[14] X. Pan and S. Lyu, "Detecting image region duplication using SIFT features," in *Acoustics Speech and Signal Processing (ICASSP), 2010 IEEE International Conference on*. IEEE, 2010, pp. 1706–1709.

[15] Y.-F. Hsu and S.-F. Chang, "Statistical fusion of multiple cues for image tampering detection," in *Asilomar Conference on Signals, Systems, and Computers*. Citeseer, 2008.

[16] S. Beeson and J. W. Mayer, *Patterns of light: chasing the spectrum from Aristotle to LEDs*. Springer Science & Business Media, 2007.

[17] M. K. Johnson and H. Farid, "Exposing digital forgeries through chromatic aberration," in *Proceedings of the 8th Workshop on Multimedia and security*. ACM, 2006, pp. 48–55.

[18] I. Yerushalmy and H. Hel-Or, "Digital image forgery detection based on lens and sensor aberration," *International Journal of Computer Vision*, vol. 92, no. 1, pp. 71–91, 2011.

[19] L. T. Van, S. Emmanuel, and M. S. Kankanhalli, "Identifying source cell phone using chromatic aberration," in *Multimedia and Expo, 2007 IEEE International Conference on*. IEEE, 2007, pp. 883–886.

[20] O. Mayer and M. C. Stamm, "Anti-forensics of chromatic aberration," in *IS&T/SPIE Electronic Imaging*. International Society for Optics and Photonics, 2015.

[21] ——, "Countering anti-forensics of lateral chromatic aberration," in *Proceedings of the 5th ACM Workshop on Information Hiding and Multimedia Security*. ACM, 2017, pp. 15–20.

[22] T. Gloe, K. Borowka, and A. Winkler, "Efficient estimation and large-scale evaluation of lateral chromatic aberration for digital image forensics," in *IS&T/SPIE Electronic Imaging*. International Society for Optics and Photonics, 2010, pp. 7541–7547.

[23] S. Zhu and K.-K. Ma, "A new diamond search algorithm for fast block-matching motion estimation," *Image Processing, IEEE Transactions on*, vol. 9, no. 2, pp. 287–290, 2000.

[24] O. Mayer and M. C. Stamm, "Improved forgery detection with lateral chromatic aberration," in *2016 IEEE International Conference on Acoustics, Speech and Signal Processing (ICASSP)*. IEEE, 2016, pp. 2024–2028.

[25] T. Gloe and R. Böhme, "The 'Dresden Image Database' for benchmarking digital image forensics," in *Proceedings of the 25th Symposium On Applied Computing (ACM SAC 2010)*, vol. 2, 2010, pp. 1585–1591.

[26] J. Shi and C. Tomasi, "Good features to track," in *Computer Vision and Pattern Recognition, 1994. Proceedings CVPR'94., 1994 IEEE Computer Society Conference on*. IEEE, 1994, pp. 593–600.

[27] J. Mallon and P. F. Whelan, "Calibration and removal of lateral chromatic aberration in images," *Pattern Recognition Letters*, vol. 28, no. 1, pp. 125–135, 2007.

[28] R. C. Gonzalez and R. E. Woods, "Digital image processing," 2008.

Owen Mayer (S'12) is a Ph.D. candidate in the Department of Electrical and Computer Engineering at Drexel University, Philadelphia, PA, USA. He received a B.S. degree in electrical engineering in 2013 from Case Western Reserve University, Cleveland, OH, USA. From 2013 to 2014 he worked as a Staff Scientist at Ocean Acoustical Services and Instrumentation Systems, Inc. in Lexington, MA, USA. Currently, he is a research assistant in the Multimedia and Information Security Lab (MISL) at Drexel University, where he is conducting research on image and multimedia forensics. His research interests include signal processing, multimedia, and machine learning.

Matthew C. Stamm (S'08–M'12) received the B.S., M.S., and Ph.D. degrees in electrical engineering from the University of Maryland at College Park, College Park, MD, USA, in 2004, 2011, and 2012, respectively.

Since 2013 he has been an Assistant Professor with the Department of Electrical and Computer Engineering, Drexel University, Philadelphia, PA, USA. He leads the Multimedia and Information Security Lab (MISL) where he and his team conduct research on signal processing, machine learning, and information security with a focus on multimedia forensics and anti-forensics.

Dr. Stamm is the recipient of a 2016 NSF CAREER Award and the 2017 Drexel University College of Engineering's Outstanding Early-Career Research Achievement Award. He was the General Chair of the 2017 ACM Workshop on Information Hiding and Multimedia Security and is the lead organizer of the 2018 IEEE Signal Processing Cup competition. He currently serves as a member of the IEEE SPS Technical Committee on Information Forensics and Security and as a member of the editorial board of IEEE SigPort. For his doctoral dissertation research, Dr. Stamm was named the winner of the Dean's Doctoral Research Award from the A. James Clark School of Engineering. While at the University of Maryland, he was also the recipient of the Ann G. Wylie Dissertation Fellowship and a Future Faculty Fellowship. Prior to beginning his graduate studies, he worked as an engineer at the Johns Hopkins University Applied Physics Lab.